J. Phys. B: At. Mol. Opt. Phys. **31** (1998) 2935–2947. Printed in the UK PII: S0953-4075(98)91980-0

Rovibrational relaxation in collisions between H_2 molecules: I. Transitions induced by ground state para-H_2

D R Flower† and E Roueff‡

† Physics Department, The University, Durham DH1 3LE, UK

‡ URA 173 (associée au CNRS et à l'Université Paris 7) et DAEC, Observatoire de Paris, F-92195 Meudon Principal Cedex, France

Received 23 February 1998

Abstract. We present the results of quantal calculations of cross sections and rate coefficients for rovibrational transitions in ortho- and para-H_2, induced by collisions with ground state para-H_2. Rovibrational levels up to $(v, J) = (3, 8)$ were included in the calculations, and rate coefficients are available for temperatures $100 \leqslant T \leqslant 6000$ K. Comparison is made with previous calculations and with measurements of the rate coefficient for vibrational relaxation $v = 1 \rightarrow 0$. Agreement is found to be good at both high and low temperatures, but the measurements exceed the calculations at intermediate temperatures. Large discrepancies are found with previous calculations, which employed a semiclassical method.

1. Introduction

Collisions between H_2 molecules are fundamentally important in both quantum mechanical and astrophysical contexts. Hydrogen is the simplest molecule, which renders possible sophisticated *ab initio* studies of the H_2–H_2 interaction potential. Furthermore, the large moment of inertia of H_2 ensures that the spacing of its rotational energy levels is wide, thereby facilitating the convergence of quantum dynamical calculations of rotational and vibrational excitation processes. Hydrogen has long been recognized as the most abundant molecule in the universe, and rovibrational transitions of H_2 have been observed for many years in a variety of stellar and interstellar objects. The recent successful launch and operation of the ISO satellite (1996, *Astron. Astrophys.* **315** (2) 'First ISO Results': special issue) has enabled a number of pure rotational transitions to be observed and given further impetus to quantitative studies of the H_2–H_2 system.

Quantum mechanical calculations of the rate coefficients for pure rotational excitation in H_2–H_2 collisions (Monchick and Schaefer 1980, Danby *et al* 1987, Flower 1998) are substantially in agreement. Such calculations require a knowledge of the intermolecular potential for the vibrationally averaged value of the internuclear separation of the H_2 molecule. Studies of rovibrationally inelastic processes, on the other hand, are more demanding. The dependence of the potential on the internuclear distance must be known, and the number of channels that has to be included when solving the collision problem is much larger. Billing and co-workers (Cacciatore *et al* 1989, Cacciatore and Billing 1992, Billing and Kolesnick 1993, Kolesnick and Billing 1993) have employed the semiclassical method in computational studies of rovibrational relaxation in H_2–H_2 collisions. The

0953-4075/98/132935+13$19.50

work of Kolesnick and Billing incorporated a fit to *ab initio* data proposed by Schwenke (1988). Schwenke's study of the H_2–H_2 hypersurface is probably the most comprehensive to date and enables the rates of vibrational relaxation to be computed for comparison with experimental data. The rate coefficient for the $v = 1 \rightarrow 0$ relaxation process has been measured in both ortho- and para-H_2, as well as normal H_2, by Audibert *et al* (1974, 1975) at low temperatures ($T < 500$ K) and, in normal hydrogen, by Dove and Teitelbaum (1974, 1979) at higher temperatures by means of shock tubes. More recently, the $v = 2 \rightarrow 1$ relaxation rate has also been measured (Kreutz *et al* 1988).

At the low energies which are relevant to many astrophysical applications, the validity of the semiclassical method of determining vibrationally inelastic cross sections is open to question. Furthermore, Kolesnick and Billing appear to have programmed erroneously Schwenke's fit to his *ab initio* data (Flower 1998). For these and other reasons, it is desirable to revisit the H_2–H_2 problem, using fully quantum mechanical methods.

2. Theory and numerical methods

The quantal scattering Colmol code of Launay (1977) was originally designed to treat rotationally inelastic collisions between molecules, as well as fine-structure excitation processes (see, for example, Flower and Launay 1977, 1985). This program has been recently modified in order to incorporate the vibrational degree of freedom and used successfully to study the rovibrational excitation of H_2 by H (Flower 1997) and He (Flower *et al* 1998). In the latter case, detailed comparison was made with cross sections obtained using the Molscat code of Hutson and Green (1995); agreement was found to be good.

The code of Launay (1977) requires the potential to be supplied in the form of the coefficients $v_{q_1q_2\mu}$ of the expansion of the intermolecular potential

$$V(\boldsymbol{r}_1, \boldsymbol{r}_2, R) = \sum_{q_1q_2\mu} v_{q_1q_2\mu}(r_1, r_2, R)\Psi_{q_1q_2\mu}(\hat{\boldsymbol{r}}_1, \hat{\boldsymbol{r}}_2) \tag{1}$$

where

$$\Psi_{q_1q_2\mu}(\hat{\boldsymbol{r}}_1, \hat{\boldsymbol{r}}_2) = \frac{4\pi}{[2(1+\delta_{\mu 0})]^{1/2}}[Y_{q_1\mu}(\hat{\boldsymbol{r}}_1)Y_{q_2-\mu}(\hat{\boldsymbol{r}}_2) + Y_{q_1-\mu}(\hat{\boldsymbol{r}}_1)Y_{q_2\mu}(\hat{\boldsymbol{r}}_2)]. \tag{2}$$

In (2), $Y_{q\mu}(\hat{\boldsymbol{r}})$ is a normalized spherical harmonic, and the polar angles $\hat{\boldsymbol{r}} = (\theta, \phi)$ are measured relative to a body-fixed coordinate frame, in which the line joining the centres of mass of the molecules is taken to be the z-axis. In practice, one of the H_2 molecules was constrained to its rovibrational ground state ($v = 0$ and $j = 1$ for ortho-H_2, $j = 0$ for para-H_2). Accordingly, we set $r_1 = 1.449\ a_0$, its expectation value in the vibrational ground state.

Schwenke (1988) calculated the interaction potential at five orientations of the H_2 internuclear axis, relative to the body-fixed z-axis, namely $[\theta_1, \theta_2, \phi_1 - \phi_2] = [0, 0, 0]$, $[\pi/2, 0, 0]$, $[0, \pi/2, 0]$, $[\pi/2, \pi/2, 0]$, $[\pi/2, \pi/2, \pi/2]$. Using his fit, we generated additional results for $[\pi/4, \pi/4, 0]$. This set of six geometries enables the six terms with $q_1, q_2 \leqslant 2$ in expansion (1) to be determined; only even values of q contribute, as H_2 is homonuclear.

Molscat does not possess an in-built facility to treat rovibrational excitation of a molecule by another molecule. However, para-H_2 in its rovibrational ground state may effectively be treated as an atom by setting the internuclear separation equal to its expectation value and averaging the potential over the orientations of the internuclear axis of the projectile molecule:

$$\bar{V}(r_1 = 1.449, \boldsymbol{r}_2, R) = \int Y_{00}^*(\hat{\boldsymbol{r}}_1) V(r_1 = 1.449, \hat{\boldsymbol{r}}_1, \boldsymbol{r}_2, R) Y_{00}(\hat{\boldsymbol{r}}_1)\, \mathrm{d}\hat{\boldsymbol{r}}_1$$
$$= \frac{1}{4\pi} \int V(r_1 = 1.449, \hat{\boldsymbol{r}}_1, \boldsymbol{r}_2, R)\, \mathrm{d}\hat{\boldsymbol{r}}_1$$
$$= \sum_{q_2} v_{q_2}(r_1 = 1.449, r_2, R)(2q_2 + 1)^{1/2} P_{q_2}(\cos\theta_2) \tag{3}$$

(cf Flower 1989). In (3), P_{q_2} is the Legendre polynomial of the order q_2. Expansion (3) will be recognized as being appropriate to the study of the rovibrational excitation of the target molecule 2 by an (effectively) atomic projectile 1.

The angular integrations in (3) were carried out numerically, using the values of the potential, V, which derive from Schwenke's fit to his *ab initio* data. This fit incorporates, at short-range, a pairwise potential, denoted V_P by Schwenke (1988), which results in contributions from anisotropies $q_1, q_2 > 2$ contributing to the fit even though, as noted above, such contributions cannot be obtained directly from the *ab initio* data. We used equation (3) to derive the coefficients $v_{q_2}(r_1 = 1.449, r_2, R)$ for $q_2 \leqslant 6$, which may be compared directly with those employed in our previous study of He–H_2 scattering (Flower *et al* 1998). We note that ground-state para-H_2 has often been assumed to behave similarly to He in molecular collision processes.

In figure 1, we compare the relative anisotropies of the matrix elements

$$y_{q_2}(v_2 = 1 j_2, v_2' = 0 j_2' | R) = (2q_2 + 1)^{1/2} \int \chi^*(v_2 = 1 j_2 | r_2) v_{q_2}(r_1 = 1.449, r_2, R)$$
$$\times \chi(v_2' = 0 j_2' | r_2)\, \mathrm{d}r_2$$

which couple the $v_2 = 1$ and 0 vibrational manifolds; in the harmonic oscillator approximation, these matrix elements are independent of j_2. Plotted are the ratios of y_4/y_2 and y_6/y_2, for both the H_2–ground-state para-H_2 and H_2–He interactions.

We see from figure 1 that ground-state para-H_2 and He exhibit qualitatively different behaviour. In the case of He, the relative anisotropies decrease with R up to about $6a_0$, where y_2 changes sign. For ground-state para-H_2, on the other hand, not only do the y_4 and y_6 matrix elements have the opposite sign from y_2 at small R, but the absolute magnitudes of the ratios y_4/y_2 and y_6/y_2 *increase* with R, i.e. the interaction becomes *more* anisotropic as the intermolecular distance increases. We consider this behaviour to be surprising to the point of being questionable. We suggest that the fitting procedure adopted by Schwenke (1988) is responsible, in particular the technique used to correct the pairwise potential, V_P (cf equation (16) of Schwenke's paper). The correction factor was determined by comparing the fit to the short range potential with the *ab initio* data for the five geometries at which the latter were calculated. Whilst this procedure is perhaps reasonable for terms $q_1, q_2 \leqslant 2$, we believe that it may distort results for $q_1, q_2 > 2$. Accordingly, we have retained only those terms with $q_1, q_2 \leqslant 2$ in the calculations reported below.

Colmol scattering calculations require the matrix elements of the vibrational eigenfunctions, $\chi(r)$,

$$y_{q_1 q_2 \mu}(v_2 j_2, v_2' j_2' | R) = \int \chi^*(v_2 j_2 | r_2) v_{q_1 q_2 \mu}(r_1 = 1.449, r_2, R) \chi(v_2' j_2' | r_2)\, \mathrm{d}r_2. \tag{4}$$

(When expansion (3) is used, $q_1 = \mu = 0$.) The vibrational wavefunctions were assumed to be harmonic oscillator eigenfunctions (and hence independent of j_2), with parameters appropriate to H_2 (Eastes and Secrest 1972). However, experimental values were adopted for the corresponding eigenenergies (Dabrowski 1984).

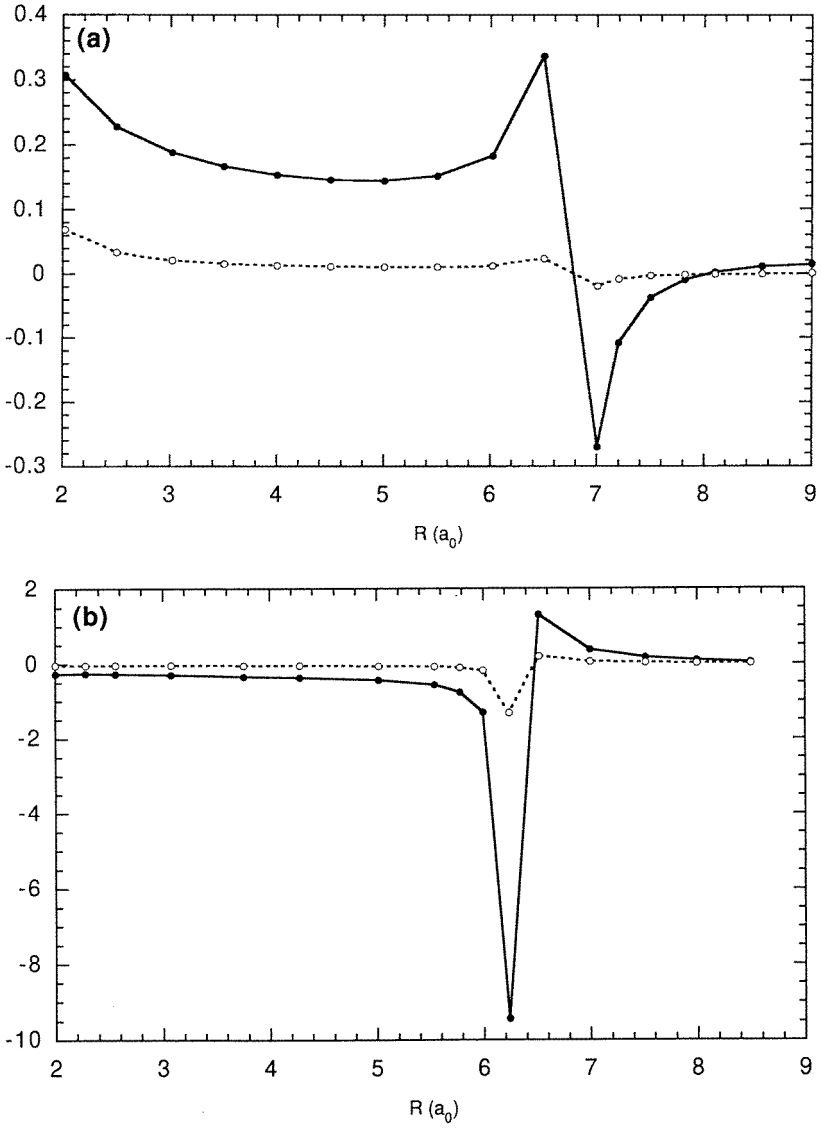

Figure 1. Relative anisotropies of the matrix elements coupling the $v = 1$ and 0 manifolds of H_2: (*a*) H_2–He potential used by Flower *et al* (1998); (*b*) H_2–ground-state para-H_2 potential derived here (see text, section 2). The full curves are the ratios y_4/y_2, the broken curves y_6/y_2 (see text, section 2).

The set of coupled differential equations which has to be solved may be written in the form

$$\left[-\frac{\mathrm{d}^2}{\mathrm{d}R^2}+\frac{l(l+1)}{R^2}-k^2_{v_2j_2j_1}\right]F(v_2j_2j_1j_{12}lJ|R) +2m\sum_{v_2'j_2'j_1'j_{12}'l'}V_J(v_2j_2j_1j_{12}l,v_2'j_2'j_1'j_{12}'l'|R)F(v_2'j_2'j_1'j_{12}'l'J|R)=0 \qquad (5)$$

where R is the distance between the centres of mass of the molecules and m is the reduced

mass; atomic units are used. In (5), v and j are the vibrational and rotational quantum numbers and $\boldsymbol{j}_{12} = \boldsymbol{j}_1 + \boldsymbol{j}_2$; l is the quantum number pertaining to the relative angular momentum of the two molecules, and $\boldsymbol{J} = \boldsymbol{j}_{12} + \boldsymbol{\ell}$ is the total angular momentum of the system; $k_{v_2 j_2 j_1}$ is the wavenumber in the centre-of-mass coordinate system, relative to level $v_2 j_2 j_1$ of the bimolecular system. The potential matrix element, $V_J(R)$, may be expressed as

$$V_J(v_2 j_2 j_1 j_{12} l, v_2' j_2' j_1' j_{12}' l' | R) = \sum_{q_1 q_2 \mu} c_{q_1 q_2 \mu}(j_2 j_1 j_{12} l, j_2' j_1' j_{12}' l'; J) y_{q_1 q_2 \mu}(v_2 j_2, v_2' j_2' | R) \qquad (6)$$

where $c_{q_1 q_2 \mu}$ is an algebraic coefficient. In practice, the scattering equations are solved in the body-fixed frame; a rotation into the space-fixed frame is performed in order to extract the scattering matrix and hence the cross sections (Launay 1977).

In our previous study of He–H_2 scattering (Flower *et al* 1998), rovibrational levels of H_2 up to approximately 20 000 K, relative to the $(v_2, j_2) = (0, 0)$ state, were included in the calculations, i.e. up to (3, 7) in ortho-H_2 and (3, 8) in para-H_2. This same basis has been used here to generate the results for excitation by para-$H_2(j_1 = 0)$. For the case of excitation by ortho-$H_2(j_1 = 1)$, this basis generates over 500 coupled equations for given values of the total angular momentum J and the total parity. Although the calculations are very computer-time consuming, we have chosen to solve the coupled equations without further approximations in order to provide benchmark results for this system; these results will be presented subsequently. In the meantime, and in order to establish the dependence, at low temperatures, of the rate coefficient for vibrational relaxation on the rotational state of the projectile molecule (para-$H_2(j_1 = 0)$ or ortho-$H_2(j_1 = 1)$), we have performed additional calculations, with para-H_2 as the target molecule, using a smaller basis of up to $(v_2, j_2) = (1, 8)$, corresponding to an excitation energy of 11 522 K relative to the ground rovibrational state.

3. Results

Cross sections for para-H_2 were calculated at a barycentric collision energy $E = 10\,000$ K, using both the Colmol and Molscat collision codes, as described in the previous section. Both the hybrid modified log-derivative/Airy propagator (Alexander and Manolopoulos 1987) and the R-matrix propagator (Stechel *et al* 1978) methods in Molscat were used, with identical results. At this energy, the cross sections agreed with those generated by Colmol to within, typically, 10–20%. Although satisfactory, this level of agreement is worse than was achieved in the analogous calculations for H_2–He scattering (Flower *et al* 1998), where cross sections were reproducible to within a few per cent. We believe that the reason for the poorer agreement in this case is that the comparison is less rigorous. The Colmol program uses the potential in the form (1) above, whereas Molscat uses the potential in the form (3). When performing the angular integrations in (3), the fit to the potential is sampled at the quadrature points, whose number considerably exceeds the number of geometries (five) from which the fit is derived, as noted above. It follows that the potentials (1) and (3) are not strictly equivalent, even when the restriction $q_1, q_2 \leqslant 2$ is applied.

At lower collision energies, but above the $v = 1$ threshold at approximately 6000 K, the sums of vibrationally inelastic cross sections, $\sum_{j'} \sigma(v = 1 j \rightarrow v' = 0 j')$, obtained using the two codes showed a similar level of agreement, although discrepancies in individual cross sections tended to increase. Once again, we attribute these differences to the forms of the potential rather than to the defects in either collision code, both of which have been extensively tested on other systems. In any case, the reproducibility of the sums

of vibrationally inelastic cross sections ensures that the conclusions reached below, when comparing the vibrational relaxation rate coefficients with measurements, remain valid. The rest of the discussion will be based on results obtained with the Colmol code.

Tables 1 and 2 present the values of the rate coefficients for selected transitions between levels of the $v = 0$, 1 and 2 states of para- and ortho-H_2 at three kinetic temperatures, $T = 1000$, 2000 and 4500 K; for purposes of comparison, the latter were chosen to be the same as in the studies of rovibrational transitions in H_2 induced by collisions with H or He (Flower 1997, Flower *et al* 1998). These results refer to excitation by ground state para-H_2, as already noted above. The rate coefficients, $q(T)$, for de-excitation were calculated from

$$q(T) = \left(\frac{8kT}{\pi m}\right)^{1/2} \int_0^\infty Q(x) x \mathrm{e}^{-x}\, \mathrm{d}x \tag{7}$$

in which $Q(x)$ is the de-excitation cross section and $x = E/kT$; m is the reduced mass of the H_2–H_2 system and E the barycentric collision energy, relative to the initial (upper) level. The integral was evaluated numerically, using a trapezoidal rule on a fine grid of the integration variable, x; $Q(x)$ was generated at the grid points by cubic spline interpolation of its computed values. Rate coefficients for excitation, also given in table 1, were obtained from the detailed balance relation

$$(2J+1) q_{vJ \to v'J'}(T) = (2J'+1) q_{v'J' \to vJ}(T) \exp[-(E_{v'J'} - E_{vJ})/kT] \tag{8}$$

(as reference to the total angular momentum of the bimolecular system is no longer required, we shall henceforth use the conventional spectroscopic symbol (upper case) J to identify the angular momentum of the H_2 molecule).

In table 3, we present the computed values of the relaxation rate coefficient in the temperature range $100 \leqslant T \leqslant 3000$ K. It has been evaluated as

$$q_{v=1\to 0}(T) = \frac{\sum_{JJ'} n(v=1, J) q(v=1, J \to v'=0, J')}{\sum_J n(v=1, J)} \tag{9}$$

where q denotes a rate coefficient for de-excitation from $v = 1$, J to $v' = 0$, J' and $n(v = 1, J)$ is the population of the upper level of the collision-induced transition. For the latter, we assume a Boltzmann distribution to be established amongst the rotational levels of the $v = 1$ vibrational state.

In table 3, the calculated values of $q_{v=1\to 0}(T)$ are compared with the experimental results of Audibert *et al* (1974, 1975) and, at higher temperatures ($T > 1000$ K), with the shock tube measurements of Dove and Teitelbaum (1974). At low ($T = 100$ K) and high ($T = 3000$ K) temperatures, agreement between theory and experiment is good. However, the theoretical results fall below the values measured at intermediate temperatures, the discrepancy attaining an order of magnitude at 500 K. The difference between the rate coefficients for relaxation of ortho- and para-H_2 becomes significant only at low temperatures, $T < 200$ K, where both the calculated and measured values for ortho-H_2 exceed those for para-H_2. Similarly, the rate coefficient for vibrational relaxation $v = 2 \to 1$ calculated at $T = 300$ K (5×10^{-17} cm^3 s^{-1}) is an order of magnitude smaller than the lower bound of the measurement (6×10^{-16} cm^3 s^{-1}) by Kreutz *et al* (1988). These conclusions contrast with those drawn by Flower *et al* (1998) regarding the vibrational relaxation of H_2 in He, where the theoretical results exceed the values measured, over the same temperature range, but by no more than a factor 2.

Comparison may also be made with the semiclassical calculations of the $v = 1 \to 0$ vibrational relaxation rate coefficient, as performed by Kolesnick and Billing (1993) and Billing and Kolesnick (1993). In the former, Kolesnick and Billing used, as we do, the fit

Table 1. Rate coefficients (in units of $cm^3\ s^{-1}$) for rovibrational transitions in para-H_2, induced by collisions with ground-state para-H_2. Results are given at three values of the kinetic temperature, T. The values of (v, J) which label the columns denote the initial state, those which label the rows denote the final state. Thus, the upper right triangle of each matrix refers to collisional de-excitation, and the lower left triangle to excitation (obtained using the detailed balance relation, equation (8)). More extensive results are available electronically from the CCP7 server (ftp://ccp7.dur.ac.uk/ccp7/).

$T = 1000$ K

	(0, 0)	(0, 2)	(0, 4)	(0, 6)	(0, 8)	(1, 0)	(1, 2)	(1, 4)	(0, 10)	(1, 6)	(1, 8)	(2, 0)	(0, 12)	(2, 2)
(0, 0)	1.9D−09	6.0D−12	5.5D−14	4.1D−16	2.5D−18	1.0D−16	1.0D−17	2.2D−18	1.3D−20	1.7D−19	5.8D−21	6.2D−19	6.2D−23	5.5D−20
(0, 2)	1.8D−11	2.1D−09	4.7D−12	3.3D−14	2.1D−16	3.7D−16	1.9D−16	2.0D−17	1.2D−18	2.2D−18	1.2D−19	2.5D−19	6.1D−21	7.6D−19
(0, 4)	9.3D−14	6D−12	2.1D−09	1.8D−12	1.1D−14	2.1D−16	9.6D−16	2.8D−16	6.3D−17	2.3D−17	1.5D−18	1.7D−19	3.5D−19	2.7D−19
(0, 6)	1.7D−16	4.4D−15	4.4D−13	2.1D−09	7.1D−13	1.5D−17	1.8D−16	3.2D−15	3.3D−15	4.2D−16	2.3D−17	2.3D−19	1.8D−17	6.5D−19
(0, 8)	1.3D−19	3.4D−18	3.2D−16	8.8D−14	2.1D−09	2.1D−19	4.1D−18	2.0D−16	3.1D−13	1.0D−14	5.9D−16	4.1D−20	1.2D−15	3.5D−19
(1, 0)	2.5D−19	3.1D−19	3.2D−19	9.6D−20	1.1D−20	2.1D−09	7.6D−12	8.6D−14	6.4D−22	7.8D−16	5.6D−18	4.4D−16	1.8D−23	6.7D−17
(1, 2)	8.0D−20	4.8D−19	4.5D−18	3.4D−18	6.3D−19	2.4D−11	2.0D−09	6.1D−12	4.5D−20	5.3D−14	4.1D−16	1.4D−15	1.5D−21	8.0D−16
(1, 4)	9.9D−21	3.1D−20	7.6D−19	3.7D−17	1.9D−17	1.6D−13	3.6D−12	2.1D−09	1.7D−18	2.5D−12	1.8D−14	8.2D−16	6.4D−20	3.3D−15
(0, 10)	4.7D−23	1.4D−21	1.3D−19	3.0D−17	2.2D−14	9.1D−22	2.1D−20	1.3D−18	2.1D−09	1.8D−16	3.1D−14	1.3D−21	1.6D−13	2.0D−20
(1, 6)	2.0D−22	8.7D−22	1.6D−20	1.3D−18	2.5D−16	3.7D−16	8.3D−15	6.7D−13	6.2D−17	2.1D−09	1.0D−12	6.4D−17	2.4D−18	6.3D−16
(1, 8)	9.7D−25	6.7D−24	1.5D−22	9.4D−21	2.0D−18	3.8D−19	8.9D−18	6.7D−16	1.5D−15	1.4D−13	2.1D−09	1.0D−18	1.2D−16	1.7D−17
(2, 0)	5.5D−24	7.5D−25	8.7D−25	5.0D−24	7.2D−24	1.6D−18	1.6D−18	1.6D−18	3.2D−24	4.7D−19	5.4D−20	2.1D−09	4.2D−25	9.5D−12
(0, 12)	1.0D−26	3.3D−25	3.4D−23	7.4D−21	3.8D−18	1.2D−24	3.1D−23	2.3D−21	7.1D−15	3.3D−19	1.2D−16	7.7D−24	2.0D−09	1.6D−22
(2, 2)	1.5D−24	7.0D−24	4.6D−24	4.5D−23	1.9D−22	7.5D−19	2.9D−18	2.0D−17	1.5D−22	1.5D−17	2.7D−18	3.0D−11	2.8D−23	1.9D−09

Table 1. (Continued)

$T = 2000$ K

	(0, 0)	(0, 2)	(0, 4)	(0, 6)	(0, 8)	(1, 0)	(1, 2)	(1, 4)	(0, 10)	(1, 6)	(1, 8)	(2, 0)	(0, 12)	(2, 2)
(0, 0)	2.6D−09	1.5D−11	2.8D−13	4.7D−15	6.4D−17	2.3D−15	4.6D−16	9.9D−17	7.0D−19	9.4D−18	4.7D−19	4.1D−18	6.3D−21	1.1D−18
(0, 2)	5.6D−11	2.7D−09	1.4D−11	2.4D−13	3.5D−15	6.7D−15	4.4D−15	8.7D−16	4.4D−17	1.2D−16	8.3D−18	9.3D−18	4.5D−19	7.7D−18
(0, 4)	1.1D−12	1.4D−11	2.7D−09	8.2D−12	1.2D−13	4.9D−15	1.3D−14	5.9D−15	1.6D−15	9.2D−16	8.6D−17	7.2D−18	1.8D−17	1.4D−17
(0, 6)	1.1D−14	1.4D−13	4.8D−12	2.7D−09	4.2D−12	6.7D−16	3.9D−15	3.4D−14	5.1D−14	8.5D−15	9.3D−16	1.2D−17	6.4D−16	2.0D−17
(0, 8)	5.9D−17	8.4D−16	2.8D−14	1.7D−12	2.7D−09	2.8D−17	2.5D−16	4.3D−15	2.3D−12	9.0D−14	1.2D−14	3.3D−18	2.3D−14	1.5D−17
(1, 0)	1.1D−16	8.7D−17	6.3D−17	1.5D−17	1.5D−18	2.7D−09	1.8D−11	4.1D−13	8.7D−20	8.1D−15	1.3D−16	8.9D−15	2.9D−21	2.1D−15
(1, 2)	9.0D−17	2.2D−16	6.5D−16	3.4D−16	5.4D−17	7.0D−11	2.7D−09	1.8D−11	4.0D−18	3.6D−13	6.3D−15	2.2D−14	1.7D−19	1.7D−14
(1, 4)	2.0D−17	4.5D−17	3.1D−16	3.0D−15	9.5D−16	1.7D−12	1.9D−11	2.7D−09	9.8D−17	1.1D−11	1.8D−13	1.7D−14	5.1D−18	3.8D−14
(0, 10)	1.9D−19	3.1D−18	1.1D−16	6.1D−15	6.7D−13	4.7D−19	5.6D−18	1.3D−16	2.8D−09	4.3D−15	2.3D−13	2.4D−19	1.3D−12	1.9D−18
(1, 6)	1.2D−18	3.7D−18	3.0D−17	4.7D−16	1.2D−14	2.0D−14	2.3D−13	6.6D−12	2.0D−15	2.7D−09	5.7D−12	2.5D−15	1.3D−16	1.3D−14
(1, 8)	2.5D−20	1.1D−19	1.2D−18	2.2D−17	7.0D−16	1.4D−16	1.7D−15	4.8D−14	4.5D−14	2.4D−12	2.8D−09	1.2D−16	3.3D−15	9.5D−16
(2, 0)	1.2D−20	7.1D−21	5.5D−21	1.6D−20	1.1D−20	5.3D−16	3.3D−16	2.4D−16	2.6D−21	6.0D−17	6.6D−18	2.7D−09	3.0D−22	2.2D−11
(0, 12)	4.0D−22	7.4D−21	3.0D−19	1.8D−17	1.6D−15	3.7D−21	5.4D−20	1.6D−18	3.1D−13	6.6D−17	3.9D−15	6.5D−21	2.7D−09	7.4D−20
(2, 2)	1.3D−20	2.4D−20	4.4D−20	1.0D−19	2.0D−19	5.0D−16	1.0D−15	2.2D−15	8.3D−20	1.2D−15	2.1D−16	8.6D−11	1.4D−20	2.7D−09

$T = 4500$ K

	(0, 0)	(0, 2)	(0, 4)	(0, 6)	(0, 8)	(1, 0)	(1, 2)	(1, 4)	(0, 10)	(1, 6)	(1, 8)	(2, 0)	(0, 12)	(2, 2)
(0, 0)	3.6D−09	3.7D−11	1.6D−12	6.5D−14	2.2D−15	5.0D−14	1.3D−14	3.4D−15	5.9D−17	5.3D−16	5.0D−17	1.9D−16	1.4D−18	9.3D−17
(0, 2)	1.6D−10	3.7D−09	4.5D−11	1.8D−12	6.9D−14	1.2D−13	9.9D−14	2.6D−14	2.2D−15	4.9D−15	6.1D−16	6.6D−16	5.8D−17	4.8D−16
(0, 4)	1.0D−11	6.2D−11	3.7D−09	3.4D−11	1.3D−12	1.1D−13	1.8D−13	1.2D−13	4.5D−14	2.8D−14	4.1D−15	5.0D−16	1.4D−15	8.3D−16
(0, 6)	3.9D−13	2.5D−12	3.3D−11	3.8D−09	2.3D−11	2.8D−14	8.5D−14	3.5D−13	7.8D−13	1.6D−13	3.0D−14	7.1D−16	2.6D−14	8.5D−16
(0, 8)	1.0D−14	7.2D−14	9.5D−13	1.8D−11	3.8D−09	3.1D−15	1.4D−14	9.5D−14	1.6D−11	7.5D−13	2.2D−13	3.1D−16	4.8D−13	7.7D−16
(1, 0)	1.3D−14	7.1D−15	4.6D−15	1.2D−15	1.8D−16	3.6D−09	4.3D−11	2.2D−12	1.5D−17	9.8D−14	3.6D−15	1.4D−13	8.6D−19	4.4D−14
(1, 2)	1.5D−14	2.6D−14	3.4D−14	1.7D−14	3.5D−15	1.9D−10	3.7D−09	5.3D−11	3.9D−16	2.5D−12	1.1D−13	3.4D−13	2.8D−17	3.0D−13
(1, 4)	5.7D−15	9.8D−15	3.3D−14	9.7D−14	3.4D−14	1.4D−11	7.5D−11	3.7D−09	5.3D−15	4.1D−11	1.8D−12	3.1D−13	5.0D−16	4.7D−13
(0, 10)	1.8D−16	1.5D−15	2.2D−14	4.0D−13	1.0D−11	1.7D−16	1.0D−15	9.7D−15	3.8D−09	1.0D−13	1.5D−12	5.0D−17	1.1D−11	1.9D−16
(1, 6)	8.8D−16	1.8D−15	7.5D−15	4.5D−14	2.7D−13	6.1D−13	3.5D−12	4.0D−11	5.7D−14	3.8D−09	2.8D−11	9.0D−14	6.8D−15	2.4D−13
(1, 8)	6.6D−17	1.8D−16	8.8D−16	6.5D−15	6.1D−14	1.8D−14	1.2D−13	1.4D−12	6.5D−13	2.3D−11	3.8D−09	1.1D−14	8.4D−14	4.3D−14
(2, 0)	1.4D−17	1.1D−17	6.1D−18	8.9D−18	5.0D−18	4.1D−14	2.2D−14	1.4D−14	1.2D−18	4.1D−15	6.4D−16	3.6D−09	2.1D−19	4.9D−11
(0, 12)	2.4D−18	2.3D−17	3.9D−16	7.7D−15	1.8D−13	5.7D−18	4.2D−17	5.2D−16	6.3D−12	7.3D−15	1.1D−13	5.0D−18	3.8D−09	2.7D−17
(2, 2)	3.2D−17	3.6D−17	4.5D−17	4.8D−17	5.6D−17	5.7D−14	8.6D−14	9.6D−14	2.1D−17	5.0D−14	1.1D−14	2.2D−10	5.1D−18	3.7D−09

Table 2. As table 1, but for transitions in ortho-H_2 induced in collisions with ground-state para-H_2.

$T = 1000$ K														
	(0, 1)	(0, 3)	(0, 5)	(0, 7)	(1, 1)	(1, 3)	(0, 9)	(1, 5)	(0, 11)	(1, 7)	(2, 1)	(2, 3)	(1, 9)	(0, 13)
(0, 1)	3.7D−10	6.3D−12	5.0D−14	3.4D−16	1.6D−16	1.9D−17	1.9D−18	2.6D−18	1.0D−20	1.6D−19	7.3D−19	7.8D−20	5.0D−21	4.7D−23
(0, 3)	6.4D−12	2.1D−09	3.0D−12	1.9D−14	5.6D−16	2.2D−16	1.2D−16	2.2D−17	6.5D−19	1.8D−18	2.2D−19	7.5D−19	8.4D−20	3.4D−21
(0, 5)	1.8D−14	1.1D−12	2.1D−09	1.1D−12	1.7D−16	1.8D−15	5.9D−15	3.5D−16	3.4D−17	2.3D−17	3.0D−19	4.1D−19	1.2D−18	1.9D−19
(0, 7)	2.0D−17	1.1D−15	1.9D−13	2.1D−09	7.1D−18	1.9D−16	4.6D−13	5.8D−15	1.9D−15	5.0D−16	2.5D−19	1.5D−18	2.2D−17	1.0D−17
(1, 1)	3.9D−19	1.4D−18	1.2D−18	3.0D−19	2.1D−09	8.2D−12	2.7D−20	8.0D−14	1.2D−21	6.5D−16	6.8D−16	1.2D−16	4.5D−18	2.4D−23
(1, 3)	5.1D−20	5.9D−19	1.3D−17	8.5D−18	8.6D−12	2.1D−09	1.1D−18	4.1D−12	5.8D−20	3.2D−14	2.0D−15	9.4D−16	2.3D−16	1.4D−21
(0, 9)	1.1D−20	6.5D−19	9.3D−17	4.3D−14	6.0D−20	2.3D−18	2.1D−09	2.0D−16	2.2D−13	1.8D−14	2.6D−20	4.8D−19	7.0D−16	7.3D−16
(1, 5)	2.6D−21	2.2D−20	9.8D−19	9.7D−17	3.2D−14	1.6D−12	3.7D−17	2.1D−09	2.1D−18	1.6D−12	6.4D−16	5.7D−15	1.0D−14	5.9D−20
(0, 11)	3.2D−24	2.1D−22	3.0D−20	1.0D−17	1.5D−22	7.0D−21	1.2D−14	6.7D−19	2.1D−09	1.5D−16	4.3D−22	1.5D−20	5.4D−14	1.2D−13
(1, 7)	3.1D−23	3.4D−22	1.2D−20	1.6D−18	4.9D−17	2.3D−15	6.1D−16	3.0D−13	9.1D−17	2.1D−09	2.9D−17	6.5D−16	6.6D−13	2.5D−18
(2, 1)	6.6D−24	2.0D−24	7.5D−24	3.8D−23	2.4D−18	6.7D−18	4.1D−23	5.7D−18	1.2D−23	1.4D−18	2.1D−09	1.0D−11	1.3D−19	1.1D−24
(2, 3)	7.6D−25	7.3D−24	1.1D−23	2.5D−22	4.7D−19	3.5D−18	8.4D−22	5.5D−17	4.5D−22	3.3D−17	1.1D−11	2.1D−09	4.5D−18	6.6D−23
(1, 9)	1.0D−25	1.7D−24	6.8D−23	7.4D−21	3.6D−20	1.8D−18	2.5D−18	2.1D−16	3.5D−15	7.1D−14	2.9D−19	9.3D−18	2.1D−09	1.4D−16
(0, 13)	5.6D−28	4.0D−26	6.3D−24	2.0D−21	1.2D−25	6.3D−24	1.5D−18	7.0D−22	4.3D−15	1.6D−19	1.5D−24	8.0D−23	8.4D−17	2.1D−09

Table 2. (Continued)

$T = 2000$ K

	(0, 1)	(0, 3)	(0, 5)	(0, 7)	(1, 1)	(1, 3)	(0, 9)	(1, 5)	(0, 11)	(1, 7)	(2, 1)	(2, 3)	(1, 9)	(0, 13)
(0, 1)	1.6D−09	1.7D−11	3.0D−13	4.7D−15	3.8D−15	8.2D−16	6.0D−17	1.3D−16	6.4D−19	1.0D−17	6.9D−18	1.9D−18	4.7D−19	5.6D−21
(0, 3)	2.6D−11	2.7D−09	1.1D−11	1.7D−13	8.8D−15	5.0D−15	2.4D−15	8.9D−16	2.9D−17	1.0D−16	1.0D−17	9.0D−18	6.4D−18	3.0D−19
(0, 5)	3.5D−13	8.3D−12	2.7D−09	5.9D−12	3.9D−15	2.1D−14	7.7D−14	7.1D−15	1.0D−15	9.3D−16	1.1D−17	2.1D−17	7.3D−17	1.2D−17
(0, 7)	2.6D−15	6.2D−14	2.8D−12	2.7D−09	3.6D−16	4.1D−15	3.1D−12	5.5D−14	3.4D−14	1.0D−14	1.2D−17	4.0D−17	9.2D−16	4.1D−16
(1, 1)	1.9D−16	2.9D−16	1.7D−16	3.3D−17	2.7D−09	2.1D−11	2.9D−18	4.5D−13	1.4D−19	8.2D−15	1.5D−14	3.8D−15	1.2D−16	3.8D−21
(1, 3)	6.4D−17	2.6D−16	1.4D−15	5.9D−16	3.3D−11	2.7D−09	7.6D−17	1.4D−11	4.8D−18	2.6D−13	2.7D−14	1.9D−14	4.4D−15	1.6D−19
(0, 9)	1.1D−17	3.0D−16	1.3D−14	1.1D−12	1.1D−17	1.8D−16	2.7D−09	4.4D−15	1.7D−12	1.5D−13	2.2D−18	2.0D−17	1.4D−14	1.6D−14
(1, 5)	7.9D−18	3.6D−17	3.8D−16	6.1D−15	5.4D−13	1.1D−11	1.4D−15	2.7D−09	1.2D−16	7.8D−12	1.3D−14	5.9D−14	1.2D−13	4.6D−18
(0, 11)	3.1D−20	9.4D−19	4.3D−17	3.1D−15	1.4D−19	3.0D−18	4.5D−13	9.4D−17	2.7D−09	4.1D−15	1.3D−19	1.9D−18	3.6D−13	1.0D−12
(1, 7)	3.2D−19	2.0D−18	2.5D−17	5.7D−16	5.1D−15	1.0D−13	2.4D−14	3.9D−12	2.6D−15	2.7D−09	1.4D−15	1.3D−14	4.2D−12	1.2D−16
(2, 1)	2.1D−20	2.0D−20	3.0D−20	6.7D−20	8.7D−16	1.0D−15	3.6D−20	6.4D−16	7.7D−21	1.3D−16	2.7D−09	2.6D−11	1.3D−17	3.6D−22
(2, 3)	8.9D−21	2.8D−20	8.9D−20	3.5D−19	3.6D−16	1.1D−15	5.1D−19	4.6D−15	1.9D−19	2.0D−15	4.1D−11	2.7D−09	3.0D−16	1.5D−20
(1, 9)	5.3D−21	4.7D−20	7.3D−19	1.9D−17	2.7D−17	6.3D−16	8.5D−16	2.3D−14	8.3D−14	1.5D−12	4.9D−17	7.0D−16	2.7D−09	3.7D−15
(0, 13)	5.9D−23	2.0D−21	1.1D−19	7.8D−18	7.8D−22	2.1D−20	8.9D−16	7.9D−19	2.2D−13	4.2D−17	1.3D−21	3.2D−20	3.4D−15	2.8D−09

$T = 4500$ K

	(0, 1)	(0, 3)	(0, 5)	(0, 7)	(1, 1)	(1, 3)	(0, 9)	(1, 5)	(0, 11)	(1, 7)	(2, 1)	(2, 3)	(1, 9)	(0, 13)
(0, 1)	3.2D−09	4.7D−11	2.0D−12	7.7D−14	8.5D−14	2.4D−14	2.5D−15	5.1D−15	6.7D−17	6.8D−16	4.1D−16	1.7D−16	6.0D−17	1.5D−18
(0, 3)	9.0D−11	3.7D−09	4.0D−11	1.6D−12	1.4D−13	1.1D−13	5.7D−14	2.7D−14	1.7D−15	4.5D−15	6.8D−16	5.6D−16	5.2D−16	4.7D−17
(0, 5)	4.4D−12	4.5D−11	3.7D−09	2.8D−11	8.7D−14	2.4D−13	1.0D−12	1.4D−13	3.4D−14	2.9D−14	6.5D−16	1.1D−15	3.8D−15	1.0D−15
(0, 7)	1.4D−13	1.5D−12	2.4D−11	3.8D−09	1.8D−14	8.9D−14	1.9D−11	5.1D−13	6.1D−13	1.9D−13	6.9D−16	1.3D−15	3.1D−14	2.0D−14
(1, 1)	2.2D−14	1.9D−14	1.1D−14	2.5D−15	3.7D−09	5.5D−11	3.1D−16	2.7D−12	2.4D−17	1.2D−13	2.5D−13	8.3D−14	4.2D−15	1.1D−18
(1, 3)	1.2D−14	2.9D−14	5.7D−14	2.5D−14	1.1D−10	3.7D−09	4.4D−15	4.7D−11	4.6D−16	2.1D−12	4.0D−13	3.2D−13	8.8D−14	2.6D−17
(0, 9)	3.3D−15	3.9D−14	6.1D−13	1.3D−11	1.5D−15	1.1D−14	3.8D−09	1.0D−13	1.3D−11	1.1D−12	2.2D−16	9.0D−16	2.5D−13	3.8D−13
(1, 5)	3.0D−15	8.3D−15	3.8D−14	1.6D−13	6.1D−12	5.4D−11	4.5D−14	3.7D−09	6.1D−15	3.4D−11	2.5D−13	6.2D−13	1.4D−12	4.5D−16
(0, 11)	5.4D−17	7.4D−16	1.3D−14	2.6D−13	7.3D−17	7.2D−16	8.0D−12	8.4D−15	3.8D−09	1.1D−13	3.5D−17	2.3D−16	2.1D−12	9.4D−12
(1, 7)	3.6D−16	1.2D−15	6.9D−15	5.3D−14	2.3D−13	2.2D−12	4.2D−13	3.0D−11	7.0D−14	3.8D−09	5.6D−14	2.5D−13	2.4D−11	6.3D−15
(2, 1)	3.1D−17	2.6D−17	2.2D−17	2.8D−17	7.3D−14	5.8D−14	1.2D−17	3.2D−14	3.3D−18	8.1D−15	3.7D−09	6.4D−11	1.2D−15	1.7D−19
(2, 3)	2.5D−17	4.3D−17	7.3D−17	1.0D−16	4.7D−14	9.3D−14	1.0D−16	1.6D−13	4.1D−17	7.1D−14	1.3D−10	3.7D−09	1.5D−14	3.2D−18
(1, 9)	2.3D−17	1.0D−16	6.7D−16	6.3D−15	6.1D−15	6.5D−14	7.2D−14	9.0D−13	9.8D−13	1.7D−11	6.1D−15	3.9D−14	3.8D−09	8.5D−14
(0, 13)	6.9D−19	1.1D−17	2.1D−16	4.8D−15	1.8D−18	2.3D−17	1.3D−13	3.4D−16	5.1D−12	5.4D−15	1.0D−18	9.5D−18	9.9D−14	3.8D−09

Table 3. Measured and computed values of the rate coefficient (in units of $cm^3\ s^{-1}$) for vibrational relaxation of $H_2(\dot{\nu} = 1)$ in collisions with H_2. For each value of the temperature, T, the upper entry is for relaxation of ortho-H_2 and the lower entry for relaxation of para-H_2. Numbers in parentheses are powers of 10.

	$q_{\nu=1\rightarrow 0}$	
T (K)	Experiment	Theory
100	5(−18)	7.9(−18)
	4(−18)	6.4(−18)
300	1(−16)	2.3(−17)
	1(−16)	2.3(−17)
500	1(−15)	1.1(−16)
	1(−15)	1.1(−16)
1000	1(−14)	3.5(−15)
		3.5(−15)
3000	5(−13)	5.4(−13)
		5.4(−13)

of Schwenke (1988) to his *ab initio* calculations of the H_2–H_2 hypersurface. The authors reported a value of the $\nu = 1 \rightarrow 0$ rate constant of 1×10^{-15} $cm^3\ s^{-1}$ at $T = 300$ K, rising to approximately 5×10^{-15} $cm^3\ s^{-1}$ at $T = 500$ K and approaching 1×10^{-13} $cm^3\ s^{-1}$ at $T = 1000$ K (see figure 3 of Kolesnick and Billing 1993). These results lie *above* the measured values, by an order of magnitude at $T = 300$ K, where they exceed the present quantal calculations by about a factor 40. Although the comparison is confused by the fact that Kolesnick and Billing (1993) appear to have programmed Schwenke's potential fit erroneously (Flower 1998), we tentatively conclude that the semiclassical method grossly overestimates the relaxation rate coefficient at such temperatures.

In a later paper, Billing and Kolesnick (1993) recalculated the rovibrational cross sections using their own fit to Schwenke's (1988) *ab initio* results, as they considered that Schwenke's fit 'was not adequate for calculation of the weak VT transition probabilities'. In this case, the computed relaxation rate coefficient was found to be substantially smaller than they had previously calculated, thereby improving the agreement with the measurements (see figure 1 of Billing and Kolesnick (1993) but note that the labelling of both the theoretical and experimental results for H_2 and D_2 has been inverted in this figure). Thus, at $T = 300$ K, the computed value of the rate coefficient (2×10^{-16} $cm^3\ s^{-1}$) was only a factor 2 above that measured. However, their calculated values remain larger than the quantal results reported here, by an order of magnitude at this temperature. In our view, the semiclassical method is unsuited to the evaluation of the rate coefficients for vibrational relaxation at such low temperatures, particularly in the case of H_2, which has a small moment of inertia and widely spaced rotational energy levels.

The results that we have presented so far relate to transitions induced by ground-state para-H_2 (the projectile). Although the similarity of the rate coefficients for vibrational relaxation of ortho- and para-H_2 (the target) suggests only a weak dependence on the rotational quantum number, we have performed additional calculations of cross sections for rovibrational transitions in para-H_2 induced in collisions with ground-state ortho-H_2. As noted in section 2 above, a smaller basis was used for these calculations, in view of their computer-time requirements.

Table 4 shows the computed values of the $\nu = 1 \rightarrow 0$ vibrational relaxation rate coefficient, obtained with the smaller basis, at $T = 100$, 300 and 500 K.

Table 4. Computed values of the rate coefficient (in units of $cm^3\ s^{-1}$) for vibrational relaxation of para-H_2 ($v = 1$) in collisions with (*a*) ground-state para-H_2 ($J = 0$) and (*b*) ground-state ortho-H_2 ($J = 1$). The smaller basis was used in these calculations. The numbers in parentheses are powers of 10.

	$q_{v=1\to0}$	
T (K)	(*a*)	(*b*)
100	6.1(−18)	6.2(−18)
300	2.0(−17)	2.3(−17)
500	1.0(−16)	1.2(−16)

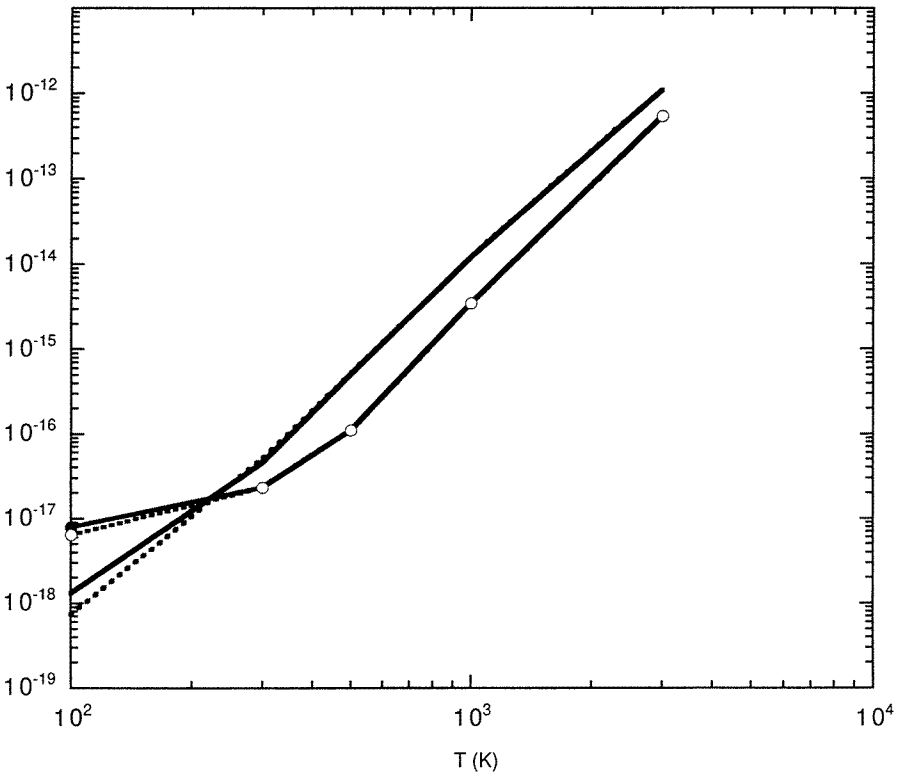

Figure 2. Computed values of the rate coefficients ($cm^3\ s^{-1}$) for the vibrational relaxation $v = 1 \to 0$ of H_2 in He (without markers) and in H_2 (with markers). Results for ortho-H_2 are shown by full curves, for para-H_2 by broken curves.

The similarity of the results in columns (*a*) and (*b*) of table 4 confirms the insensitivity of the vibrational relaxation rate coefficient to the rotational state of the projectile molecule. Furthermore, the similarity of these values to the theoretical results for para-H_2 in table 3 (the lower of the two entries for each temperature) shows that the smaller basis is adequate for determining the relaxation rate coefficient at low temperatures. We conclude that the discrepancies with the measurements, apparent in table 3, are not an artefact of the dynamical calculations but relate to the potential employed.

It is instructive to compare the rate coefficients for vibrational relaxation, $\nu = 1 \to 0$, with the corresponding results for H_2–He scattering (see figure 2). At low temperatures,

the rate coefficient for H_2–H_2 is larger than for H_2–He. The curves cross at about 230 K, and the values for He remain higher as the temperature increases further. We attribute the difference in behaviour at low temperatures to the deeper van der Waals minimum in the isotropic part of the H_2–H_2 potential: whilst the minima are shallow for both systems, that for H_2–H_2 (45 K) is about 3.5 times deeper than for H_2–He.

4. Concluding remarks

We have used fully quantal methods to calculate the cross sections, and thence the rate coefficients, for rovibrational transitions in H_2, induced by collisions with ground-state para-H_2 molecules. These results have been compared with previous semiclassical calculations and with measurements of the vibrational relaxation rate coefficient: some limited comparisons with the analogous results for H_2–He scattering have also been made. Our principal conclusions are:

- the semiclassical method is unreliable at low temperatures;
- the quantal results underestimate the measured values of the $v = 1 \rightarrow 0$ vibrational relaxation rate coefficient at intermediate temperatures ($T \approx 500$ K).

We suggest that further studies of the H_2–H_2 interaction potential, particularly of its dependence on the vibrational coordinate, are desirable.

Acknowledgments

The production computations were performed at Durham (UK) on workstations financed by grants from the Engineering and Physical Sciences Research Council. We are grateful to Dr Claude Zeippen for assistance in the early stages of this work.

References

Alexander M H and Manolopoulos D E 1987 *J. Chem. Phys.* **86** 2044
Audibert M-M, Joffrin C and Ducuing J 1974 *Chem. Phys. Lett.* **25** 158
Audibert M-M, Vilaseca R, Lukasik J and Ducuing J 1975 *Chem. Phys. Lett.* **31** 232
Billing G D and Kolesnick R E 1993 *Chem. Phys. Lett.* **215** 571
Cacciatore M and Billing G D 1992 *J. Phys. Chem.* **96** 217
Cacciatore M, Capitelli M and Billing G D 1989 *Chem. Phys. Lett.* **157** 305
Dabrowski I 1984 *Can. J. Phys.* **62** 1639
Danby G, Flower D R and Monteiro T S 1987 *Mon. Not. R. Astron. Soc.* **226** 739
Dove J E and Teitelbaum H 1974 *Chem. Phys.* **6** 431
——1979 *Chem. Phys.* **40** 87
Eastes W and Secrest D 1972 *J. Chem. Phys.* **56** 640
Flower D R 1989 *Phys. Rep.* **174** 1
——1997 *J. Phys. B: At. Mol. Opt. Phys.* **30** 3009
——1998 *Mon. Not. R. Astron. Soc.* in press
Flower D R and Launay J-M 1977 *J. Phys. B: At. Mol. Phys.* **10** 3673
——1985 *Mon. Not. R. Astron. Soc.* **214** 271
Flower D R, Roueff E and Zeippen C J 1998 *J. Phys. B: At. Mol. Opt. Phys.* **31** 1105
Hutson J M and Green S 1995 MOLSCAT Version 14 distributed by *Collaborative Computational Project 6* (Daresbury Laboratory: UK Engineering and Physical Sciences Research Council)
Kolesnick R E and Billing G D 1993 *Chem. Phys.* **170** 201
Kreutz T G, Gelfand J, Miles R B and Rabitz H 1988 *Chem. Phys.* **124** 359
Launay J-M 1977 *J. Phys. B: At. Mol. Phys.* **10** 3665
Monchick L and Schaefer J 1980 *J. Chem. Phys.* **73** 6153
Schwenke D W 1988 *J. Chem. Phys.* **89** 2076
Stechel E B, Walker R B and Light J C 1978 *J. Chem. Phys.* **69** 3518